Diamond & Related Materials 18 (2009) 1360–1368

Contents lists available at ScienceDirect

Diamond & Related Materials

journal homepage: www.elsevier.com/locate/diamond

# Corrosion behavior of amorphous carbon deposit in 0.89% NaCl by electrochemical impedance spectroscopy

D. Turcio-Ortega *, S.E. Rodil, S. Muhl

*Instituto de Investigaciones en Materiales, Universidad Nacional Autónoma de México, Ciudad Universitaria, 04510 México D.F., México*

ARTICLE INFO

*Article history:*
Received 10 March 2009
Received in revised form 8 July 2009
Accepted 19 August 2009
Available online 3 September 2009

*Keywords:*
Amorphous carbon
Corrosion
Sputtering
Biomaterials

ABSTRACT

Amorphous carbon films were deposited on SS316L substrates using a DC magnetron sputtering system, aiming at the application of the coated SS316L for biomedical implants. The biocompatibility and chemical stability of the carbon layers have been previously demonstrated. The films were deposited on top of sputtered titanium coatings introduced as a buffer layer to enhance film-substrate adhesion. The corrosion resistance of the a-C/Ti/SS316L systems was investigated by electrochemical techniques. The electrolyte used in this work was 0.89 wt.% NaCl at pH 7.4, which simulates body fluid ionic concentrations. The coated samples displayed corrosion resistance values in the saline solution much higher than the stainless steel substrates and the role of the Ti coating thickness was analysed in order to determine the optimal system for biological applications.

© 2009 Elsevier B.V. All rights reserved.

## 1. Introduction

In the biomedical area, implants of artificial joints are almost a routine surgical procedure [1]. The hip and the knee joints are the two most common replacements and have proven to be very effective in relieving pain. Moreover, the success rates are as high as 95% at least in the short time. Nowadays, the major problem of artificial joints concerns to the long-term durability: on the average, a total hip joint replacement lasts 10–15 years [2]. With many of the artificial joint recipients living longer and having a more active lifestyle, 10–15 years is no longer adequate. Many patients require a second implant or revision surgery, which is more difficult, has a much lower success rate, and has higher rates of complications. Even younger candidates who can benefit from total joint replacements have to wait until their arthritic condition is unbearable before being considered for a joint implant [3].

Among the different factors that influence the lifetime of orthopaedic implants (cup alignment, implant geometry, patient level of activity, etc.,) there are two which are specifically materials related: one is the wear of the moving parts, which leads to wear debris induced osteolysis [4]; the other is the corrosion of the implant surface, which leads to metal ions release with potential adverse effects such as toxicity, hypersensitivity and carcinogenesis [5].

Both of the above mentioned problems are mainly related to the surface of the implant, therefore a possible solution might come from surface modifications of the current materials. One of the methods for modifying surface properties is through deposition of a distinctive surface layer in the form of a coating. Amorphous carbon coatings have been proposed as possible and viable surface modification for metallic implants, since their hardness, wear resistant, low friction coefficient, biocompatibility and chemical stability have been clearly identified [6–8]. The family of "Amorphous carbon-based films" include a wide range of films having different properties, such as, diamond-like carbon (DLC) films, which are very hard and under certain environmental conditions might have friction coefficients in the $10^{-2}$ range that makes them excellent candidates for coating the moving parts of orthopaedic implants [9]. These films have been proposed to coat the counterface of the ball in hip joints; and although very successful in the lab tests, they failed during real applications due to corrosion induced wear and delamination [6]. The possible reason for this failure is the high internal stress characteristic of these DLC films. On the other hand, the less hard, graphitic-like coatings have no applications for bearings since neither the friction coefficient or wear resistance are adequate [10]. Nevertheless, during the last years, we have been investigating the osteogenesis capabilities of the graphite-like carbon (GLC) films obtaining encouraging results, which show that GLC films might be very attractive for improving the bone-implant interface, where tribology is not an issue [11,12]. A second advantage of coating the metallic implant by this inert material might be a reduction in the release of metallic ions [9,13–15]. As mentioned above, the failure of the implants is partly due to the liberation of metallic ions since the implant is subject to the harsh environment of the human body (typically oxygenated saline solution with salt content of about 0.89% at pH of 7.4). Therefore, in this work we investigated the performance of graphite-like amorphous carbon films as a corrosion resistance barrier for stainless steel substrates immersed in NaCl solutions using the electrochemical techniques.

* Corresponding author. Tel.: +52 55 56224734; fax: +52 55 56161251.
*E-mail address:* dturcio@hotmail.com (D. Turcio-Ortega).

0925-9635/$ – see front matter © 2009 Elsevier B.V. All rights reserved.
doi:10.1016/j.diamond.2009.08.013

One of the major drawbacks of depositing amorphous carbon on metals is that the film-substrate adhesion is not good enough for real applications. Many researchers have shown that this issue can be properly addressed by depositing metallic buffer layers, such as, chromium, tungsten, or titanium based films [16–19] previous to the a-C film growth. In order to address this issue, we deposited titanium buffer layers of different thicknesses between the substrate and the a-C film. Electrochemical evaluation of the Ti/a-C double-layer systems was done to select the thickness ratio (Ti/a-C) that gives a better performance.

Both, polarization curves and electrochemical impedance spectroscopy (EIS) as a function of the immersion time were used to evaluate the corrosion barrier properties of the Ti/a-C double-layer systems. Some issues concerning the corrosion properties of physical vapor deposited (PVD) coatings are the degree of porosity and the interdiffusion and adhesion of the coating-substrate interface [20]. Porosity of PVD coatings cannot be assessed by direct methods, such as, $H_2$ diffusion, optical or SEM microscopy, since the pores are usually in the nanometer scale. However, electrochemical methods can indirectly determine the presence of pores or pinholes from measurements of the through-pores in the coatings [19,20]. The presence of these through-pores can be detected since they provide a passage for the electrolyte to reach the substrate, reacting chemically or electrochemically and giving rise to measurable current signals. Moreover, the film-substrate adhesion can be qualitatively evaluated by simple observation of the no-delamination of the films after long immersion times in the electrolyte.

In this paper, we presented the electrochemical impedance analysis of a series of a-C coatings deposited on medical grade 316 L stainless steel (SS) substrates using titanium layers of different thickness as buffer layers.

## 2. Experimental

### 2.1. Substrate preparation

Stainless steel sheets (AISI 316 L) were cut into square pieces of $1 \times 1$ cm size. These 1 $cm^2$ stainless steel (SS) pieces were used as substrates. Firstly, they were polished using SiC grit up to grade 600 and then cleaned using acetone, isopropanol and deionized (DI) water in an ultrasonic bath.

### 2.2. Preparation of Ti and a-C coatings by magnetron sputtering

The titanium films were deposited directly on the SS substrate from a pure titanium target (10 cm in diameter, 99.99% pure Ti) using a magnetron sputtering system. The Argon plasma was excited by a dc-pulse source working at 250 kHz and 250 W rms-power. The deposition pressure was 4 mTorr and the Ar flux was 10 sccm, while the deposition time was changed to obtain three different thicknesses for the Ti films, as shown in Table 1. Then, the samples were transferred to another chamber, where a 240 nm carbon film was deposited using a hollow cathode (10 cm in diameter graphite target, 99.99% pure C) magnetron sputtering system under dc current conditions. The deposition conditions of the carbon film were: 250 W, 20 mTorr, 10 sccm of Ar and 450 s. For both systems the substrate holder was not cooled, therefore the substrate temperature increased according to the deposition time, reaching maximum values around 120 °C. The thicknesses of the Ti films were chosen to represent different percentages of the a-C thickness; less than 10%, half-half and more than 100%.

**Table 1**
Samples obtained by MS deposition.

| Sample Name | Thickness (nm) |
|---|---|
| SS | – |
| Ti1 | 16 |
| Ti2 | 100 |
| Ti3 | 530 |
| aCTi1 | 240 [16] + 16 (Ti) |
| aCTi2 | 240 [16] + 100 (Ti) |
| aCTi3 | 240 [16] + 530 (Ti) |

### 2.3. Electrochemical experiments

Electrochemical experiments were carried out using a standard three-electrode system where a saturated calomel electrode (SCE) was used as the reference electrode and a platinum counter electrode. The working electrodes were the a-C/Ti/SS system and Ti/SS films were evaluated in order to gain some understanding of the electrochemical process. The samples were sealed to a wall of the electrochemical cell using a Viton O'ring leaving an area of 0.15 $cm^2$ exposed to the solution.

The corrosion resistance was examined in an electrolyte of 0.89% NaCl at pH 7.4, which simulates body fluid conditions. The electrochemical impedance experiments were carried out as a function of the

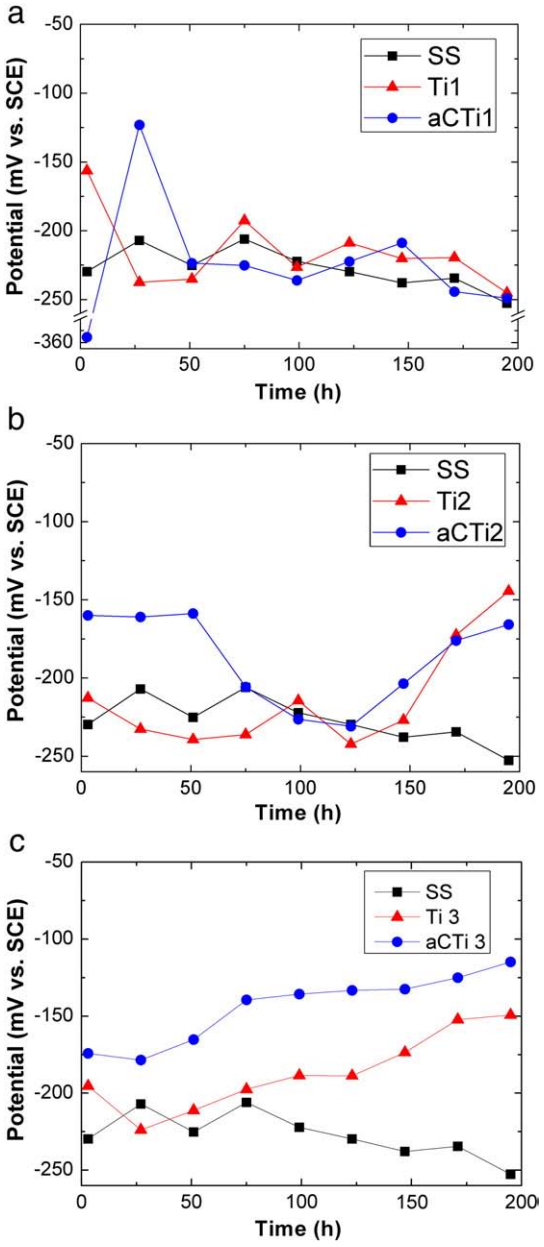


**Fig. 1.** Open circuit potential of the bare stainless steel substrate, the Ti coatings and the double-layer aCTi systems. a — OCP values of Ti1 and aCTi1 samples, b — OCP values of Ti2 and aCTi2 samples, c — OCP values of Ti3 and aCTi3 samples.

immersion time, up to 195 h and a frequency range from 10 kHz to 1 mHz. Five data points per decade were measured at amplitude of 10 mV. Polarization curves were obtained after EIS experiments, the scan rate was 0.1666 mV/s from an initial potential of −0.28 V (versus the Open Circuit Potential) to the final potential of 0.28 V. The potentiodynamic polarization curves and the EIS spectra were obtained using a Gamry Potentiostat, Framework 2004, Version 5.3.

### 2.4. Film characterization

The morphology of the substrate and the films was investigated using a scanning electron microscope (Leica, Cambridge). Raman spectroscopy of the a-C samples were recorded using an Yvon Jobin Horiba (T64000) spectrometer, equipped with a confocal microscope (Olympus, BX41) with an argon ion laser operating at 514.5 nm at a power level of 10 mW.

## 3. Results and discussion

### 3.1. Open circuit potential

Fig. 1 shows the variation of the open circuit potential (OCP) with the immersion time for the different surfaces indicated in Table 1. Fig. 1(a), (b) and (c) refers to the different Ti thicknesses; 16, 100 and 530 nm, respectively, where the signal from the SS substrate is included as reference. From these figures, it might be seen that the bare substrate showed a decrease in the OCP values as time increased, which can be associated to the pitting attack and oxide dissolution taking place at the SS surface. In Fig. 1(a), at the first hours, the OCP values for Ti1 and aCTi1 samples were different to the SS, but after 50 h of immersion, they both were very similar to the substrate. This was expected, since it corresponds to the thinnest Ti film, where a complete substrate surface coverage might not be attained yet. Fig. 1(b) shows that the aCTi2 had a higher OCP than both SS and Ti2, but there was a change around 50 h where a sudden decrement was observed, this behavior can be explained by the penetration of the solution through the open-pores of the a-C film. However, above 123 h the OCP increased again for both Ti2 and aCTi2 samples, probably due to the development of the TiOx film, either in the pure Ti film or through the pores of the aCTi2 sample. The formation of the oxide Ti film during the immersion in the NaCl electrolyte has been well documented [21]. Finally, in Fig. 1(c), it might be seen that for the thicker Ti films the OCP values increased with immersion time becoming more noble than the SS, which could be associated to a combination of the larger thickness, a better SS surface coverage and the development of a Ti-oxide film. For the aCTi3, this combination was reflected in a more noble potential along the 195 h, which also increased with time suggesting a more compact and, defect-free film. The OCP value at 195 h was −249 mV for the aCTi1 sample and become more noble as the thickness of the Ti film increased, reaching about −114.8 mV for the aCTi3.

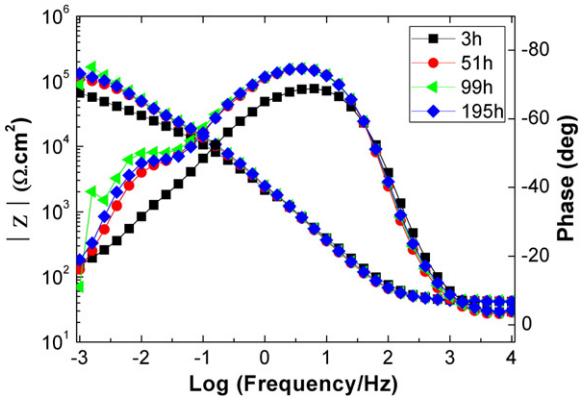


**Fig. 2.** Bode plots of the experimental data of SS as a function of immersion time. Left axis is the magnitude of the impedance and right axis is the phase angle.

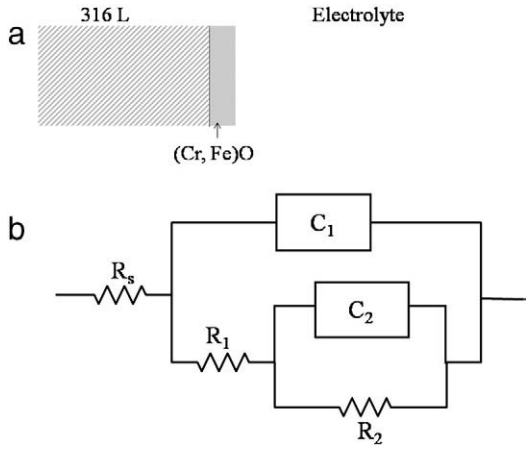


**Fig. 3.** a — Schematic representation of the bare substrate, b — EC used in the generation of the simulated data.

### 3.2. EIS

The electrochemical impedance spectra can be presented using either Nyquist or Bode representations. Bode plots includes specifically the frequency range, so it is easier to describe the different phenomena occurring at the interfaces. These phenomena can also be described using equivalent circuits, where any peak in the phase–frequency plot is associated to an RC time constant.

#### 3.2.1. SS–electrolyte interface

The EIS spectra as a function of the immersion time for the SS substrate are shown in Fig. 2 and the equivalent circuit (EC) used to

**Table 2**
Numerical results of the EIS simulations for the Ti-coated SS and, aCTi-coated SS.

| Sample | Immersion time (h) | $R_2$ $\times 10^3$ ($\Omega$ cm$^2$) | $R_1$ $\times 10^3$ ($\Omega$ cm$^2$) | $C_2$ $\times 10^{-6}$ $S*s^n$ | $n$ | $C_1$ $\times 10^{-6}$ $S*s^n$ | $m$ |
|---|---|---|---|---|---|---|---|
| SS | 3 | – | 335.3 | – | – | 18.44 | 0.7534 |
| | 51 | 616.6 | 189.4 | 29.47 | 0.8582 | 11.94 | 0.8745 |
| | 99 | 1167 | 197.1 | 20.99 | 0.8008 | 11.13 | 0.8765 |
| | 195 | 721.8 | 223.5 | 37.92 | 0.9274 | 11.82 | 0.8657 |
| Ti1 | 3 | 179.9 | 55.48 | 26.57 | 0.6387 | 14.04 | 0.7805 |
| | 51 | 669 | 234.8 | 22.56 | 0.7585 | 13.64 | 0.8089 |
| | 99 | 804.9 | 234.7 | 13.64 | 0.6674 | 13.86 | 0.8133 |
| | 195 | 744.3 | 236.6 | 34.38 | 0.8853 | 15 | 0.809 |
| Ti2 | 3 | 84.78 | 67.12 | 64.97 | 0.9298 | 36.85 | 0.8265 |
| | 51 | 76.31 | 74.42 | 80.55 | 0.9392 | 36.34 | 0.8295 |
| | 99 | 264.2 | 222.4 | 20.9 | 0.7614 | 10.62 | 0.9635 |
| | 195 | 633.1 | 420.5 | 34.45 | 0.8711 | 28.33 | 0.8499 |
| Ti3 | 3 | 258.9 | 133.4 | 172.5 | 0.9387 | 33.81 | 0.8327 |
| | 51 | 1079 | 209.4 | 63.31 | 0.8437 | 37.81 | 0.8229 |
| | 99 | 2668 | 195.6 | 60.52 | 0.8908 | 34.56 | 0.8176 |
| | 195 | 5949 | 259.7 | 52.87 | 0.9595 | 29.39 | 0.809 |
| aCTi1 | 3 | 745.6 | 59.73 | 44.6 | 0.7755 | 6 | 0.9094 |
| | 51 | 892.5 | 122.6 | 25.98 | 0.8916 | 10.09 | 0.8812 |
| | 99 | 850 | 118 | 26.31 | 0.8879 | 10.69 | 0.8859 |
| | 195 | 839.3 | 114.7 | 28.48 | 0.8839 | 10.73 | 0.8889 |
| aCTi2 | 3 | 3090 | 159.6 | 6 | 0.6897 | 10.92 | 0.7956 |
| | 51 | 889.7 | 273.2 | 21.75 | 0.8671 | 15.71 | 0.8299 |
| | 99 | 1514 | 293.7 | 26.6 | 0.8995 | 19.08 | 0.8303 |
| | 195 | 1378 | 269.2 | 31.05 | 0.9188 | 21 | 0.8295 |
| aCTi3 | 3 | – | 283.5 | – | – | 20.43 | 0.802 |
| | 51 | 4009 | 202.4 | 13.7 | 1 | 35.93 | 0.6994 |
| | 99 | 5640 | 378.4 | 9.937 | 1 | 32.54 | 0.6912 |
| | 195 | 6070 | 103.9 | 22.8 | 1 | 23.08 | 0.684 |

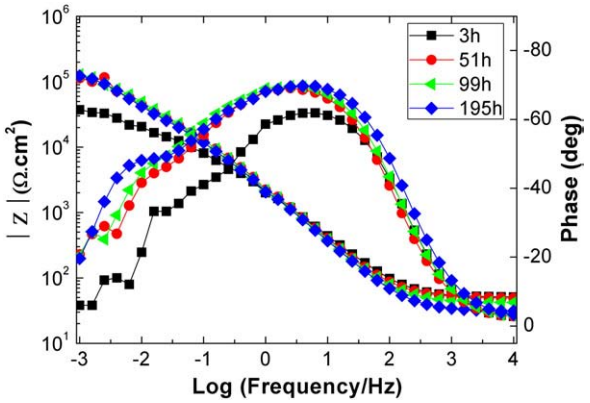


**Fig. 4.** Bode plots of the experimental data for Ti1 as a function of immersion time.

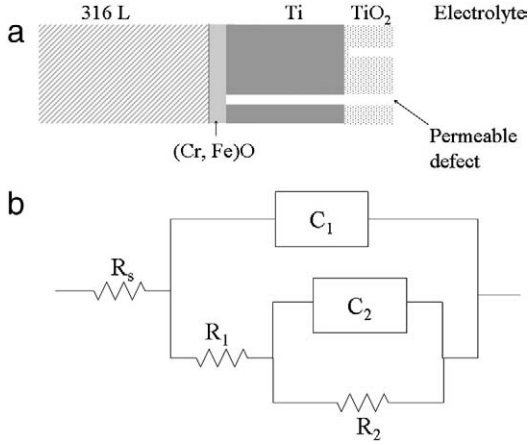


**Fig. 7.** a — Schematic representation of the Ti deposit, b — EC used in the generation of the simulated data.

model the response is shown in Fig. 3. During the first hours, a single time constant (~$10^{-1}$ Hz) in the phase angle vs. frequency plot was observed, which was modelled using a single RC circuit. However, after 51 h of immersion time, a second time constant at lower frequency was observed which is an indication of the presence of a passive film composed of chromium and iron oxide, and therefore a second RC branch has to be considered during the modeling. At the SS–electrolyte interface the upper branch of the EC contains the resistance and capacitor parameters ($R_1$, $C_1$) which are correlated to the SS surface – electrolyte interface and the parameters at the lower branch ($R_2$, $C_2$) which take in consideration the redox process that takes place in the passive layer [22]. In practice, the single capacitance were substituted by constant phase elements (CPE), in order to take into account the non-ideal capacitive behavior of the oxide–electrolyte interface. This non-ideal behavior has been attributed to surface roughness, inhomogeneous dissolution or dielectric behavior of the film [23]. Table 2 shows the numerical results of the simulations for all coatings and the substrate.

### 3.2.2. Ti-coated SS–electrolyte interface

Figs. 4, 5 and 6 show the Bode plots as a function of immersion time for the titanium coated samples. It can be seen that for all the Ti-coated samples, there was one time constant located about $10^1$ Hz, which represented the film capacitance ($C_1$) and the pore resistance ($R_1$). Slight variations were observed during the first immersion times (3h) and

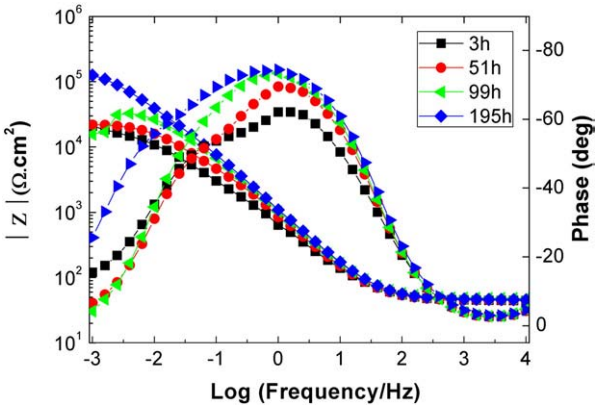


**Fig. 5.** Bode plots of the experimental data for Ti2 as a function of immersion time.

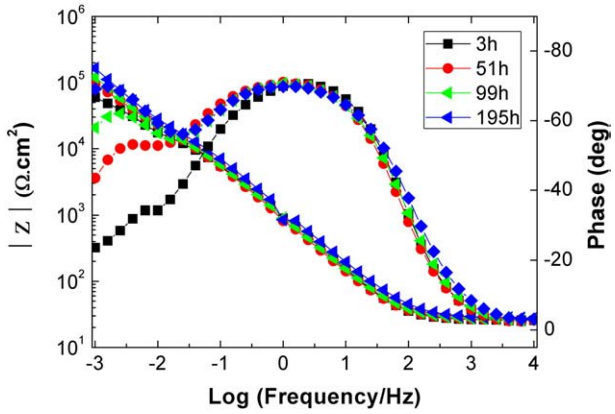


**Fig. 6.** Bode plots of the experimental data for Ti3 as a function of immersion time.

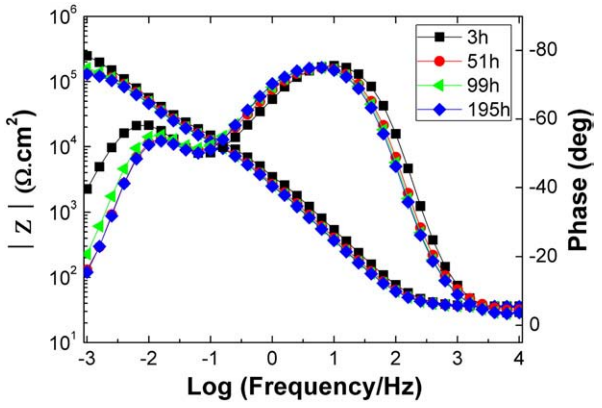


**Fig. 8.** Bode plots of the experimental data for aCTi1 as a function of immersion time.

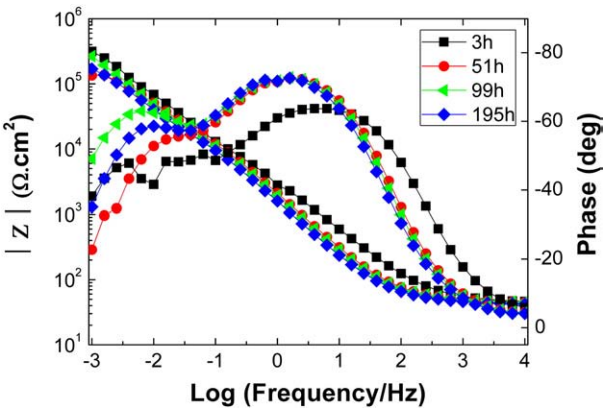


**Fig. 9.** Bode plots of the experimental data for aCTi2 as a function of immersion time.

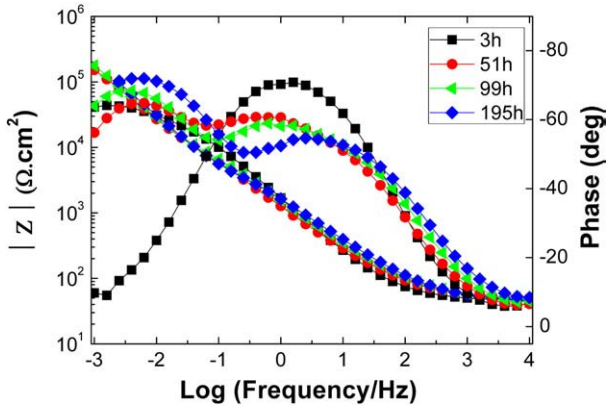


**Fig. 10.** Bode plots of the experimental data for aCTi3 as a function of immersion time.

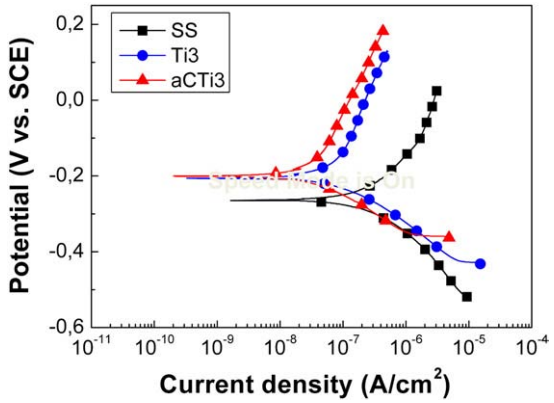


**Fig. 12.** Polarization curves for SS, Ti3 and aCTi3 in NaCl 0.89%. Scan rate was 0.1666 mV/s.

then remained similar. There was a second time constant, which appeared as the immersion time increased, located around $10^{-2}$ Hz, but its precise position and intensity varied according to the film thickness. For the thinner Ti films (Ti1 and Ti2), only a shoulder in the phase diagram can be observed but for the Ti3 film there was clearly a second peak, which intensity increased with immersion time. The equivalent circuit used to model the impedance response of the Ti films was similar to that shown in Fig. 3, but the interpretation given to the elements was slightly different, as can be seen in the schema shown in Fig. 7. It consisted of the Ti layer deposited on SS having passive chromium and iron oxide film forming the substrate–Ti film interface. Permeable defects are represented by the absence of the Ti film or pores, where the steel substrate was exposed to the electrolyte [21]. In this case, the parameters given in Table 2 correspond to the solution resistance $R_s$, $R_1$ is the pore resistance, $R_2$ is the substrate polarization resistance, $C_1$ is the coating capacitance and $C_2$ is the substrate capacitance.

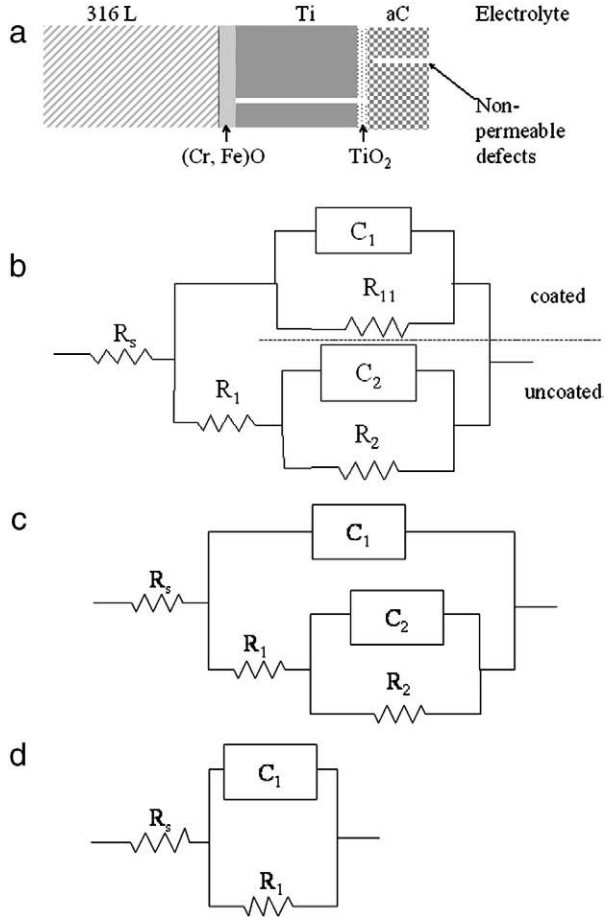


**Fig. 11.** a — Schematic representation of the Ti/a-C systems, b — EC used in the generation of the simulated data for the Ti/a-C systems, c — reduced model for the EC for the Ti/a-C systems, d — model for the aCTi3 system at 3 h of immersion time.

### 3.2.3. aCTi-coated SS–electrolyte interface

Figs. 8, 9 and 10, show the EIS spectra of the aCTi bilayers. There was a clear difference between these bilayers and the previous single Ti coatings. The phase spectra showed two time constants for the 3 different samples even at the first hours of immersion, except for the aCTi3 sample. For the aCTi1 and aCTi2 samples, there was a nearly constant high frequency peak, but the low-frequency peak associated with the permeation of the electrolyte through the pores showed an oscillatory behavior, where both frequency and intensity varied. Nevertheless, in both cases the low-frequency peak intensity was lower than the high frequency signal. For the aCTi3 sample, there was a drastic change in the response between 3 and 51 h. At 3 h only one time constant was observed and above 51 h there was a second time constant having a larger intensity than the high frequency signal. Indeed, the variation occurred since the 27 hours of immersion time (spectra not shown). The complexity of these spectra was expected due to the presence of more than two interfaces, and the fact that any of them can be reach through the film porosity, as shown schematically in Fig. 11(a). The EC for these samples at any time consist of a parallel combination of coated and uncoated areas as shown in Fig. 11(b). The EC represented in Fig. 11(b) take in consideration the solution resistance $R_s$, the resistance of the outer porous layer $R_1$, the capacitance of the outer porous layer $C_1$, the capacitance of the bilayer $C_2$, the resistance of the bilayer $R_2$ and, the resistance of the bilayer at the porous area $R_{11}$. However, for these carbon coatings $R_{11}$ was usually very large and then a simplified model can be used as shown in Fig. 11(c). In the specific case of the aCTi3 at 3 h, the contribution of SS was not important and only a small fraction of Ti was exposed to the saline solution then, the system can be represented by a simplified circuit as is shown in Fig. 11(d). In this figure, $R_s$ is the solution resistance, $C_1$ is the capacitance of the bilayer free of pores, and $R_1$ is the corrosion resistance of the whole surface averaged for the

**Table 3**
Electrochemical parameters obtained from the polarization curves.

| Sample | $E_{corr}$ V | $I_{corr}$ A/cm² | $\beta_a$ V/dec | $\beta_c$ V/dec | $R_p$ Ω·cm⁻² |
|---|---|---|---|---|---|
| SS | −0.2630 | $4.05\times10^{-7}$ | 0.2852 | 0.1892 | $1.2915\times10^{5}$ |
| Ti1 | −0.1960 | $1.07\times10^{-7}$ | 0.1677 | 0.1938 | $3.4800\times10^{5}$ |
| Ti2 | −0.2660 | $7.33\times10^{-8}$ | 0.3259 | 0.1036 | $2.5620\times10^{5}$ |
| Ti3 | −0.1950 | $1.26\times10^{-7}$ | 0.2582 | 0.1308 | $2.6670\times10^{5}$ |
| aCTi1 | −0.1950 | $1.81\times10^{-8}$ | 0.2626 | 0.1051 | $1.6950\times10^{5}$ |
| aCTi2 | −0.1450 | $8.40\times10^{-8}$ | 0.2246 | 0.1169 | $2.5650\times10^{5}$ |
| aCTi3 | −0.1970 | $3.99\times10^{-8}$ | 0.3878 | 0.1081 | $7.7715\times10^{5}$ |

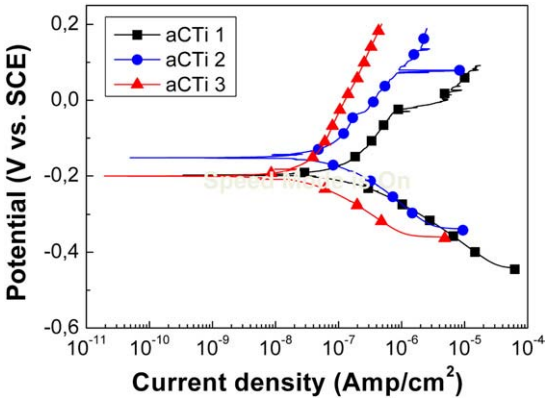


**Fig. 13.** Polarization curves for aCTi1, aCTi2 and, aCTi3 in NaCl 0.89%. Scan rate was 0.1666 mV/s.

coated and uncoated areas. This peculiar behavior might be explained as due to either the pores of the bilayer are not absolutely open, or their diameters are only big enough to allow some specific ions or molecules in the electrolyte to gradually migrate to the substrate surface [24].

Summarizing, the presence of two time constants suggest that as the immersion time increases the a-C pores permit the solution to penetrate to the Ti layer, causing an increase in the phase angle in the Bode plots at low frequencies due to the presence of Ti-oxides, which also do not let the solution to penetrate to the steel substrate.

Table 2 shows the results of the simulation process using the models mentioned above for each case.

Figs. 8, 9 and 10 also show the variation of the impedance magnitude as a function of both time and Ti thickness. The $|Z|$ values at high frequencies were very similar for all cases, and represented the solution resistance. Between $10^3$ to $10^{-1}$ Hz, the $|Z|$ values of the spectra showed a linear slope of about −1, this behavior is the characteristic response of a film with a small amount of permeable defects. At lower frequencies, the magnitude of the impedance for all samples and times was usually above $10^5\,\Omega cm^2$ with a slope similar to that of the medium frequency range, except for the aCTi3 sample where a clear saturation about $4\times10^4\,\Omega cm^2$ was observed at 3 h.

### 3.3. Polarization curves

After EIS testing, polarization curves were obtained. The electrochemical parameters obtained from the Tafel polarization curves (Fig. 12) for the uncoated and coated samples are summarized in Table 3. Fig. 12 compares the SS substrate to the Ti3 and the aCTi3 system. It shows that the uncoated substrate has a negative corrosion potential of −0.2852 V while for the coated substrate, either with Ti or a bilayer aCTi, there was a shift to the noble direction with values close to −0.2 V. From the linear part in the Tafel regime, the corrosion current density ($I_{corr}$) of $1.26\times10^{-7}$ A/cm$^2$ was determined for the Ti sample, which is lower than the $I_{corr}$ for the bare substrate. Moreover, the lower $I_{corr}$ value was obtained for the aCTi3 sample ($3.99\times10^{-8}$ A/cm$^2$). These data are proportional to the corrosion rate and confirm the larger resistance observed for the aCTi3 sample. The polarization resistance $R_p$ was calculated from the slope of the curve at the corrosion potential ($E_{corr}\pm10$ mV) and the values are shown in Table 3. It is also evident that the aCTi3 sample showed the larger polarization resistance. Finally, Fig. 13 compares the polarization curves of the three bilayers, where at the potential of −0.02 V for the aCTi1 sample a change in the current density took place from $10^{-6}$ to $10^{-5}$ A/cm$^2$ as part of a delamination process which was later observed in SEM. The aCTi2 and aCTi3 samples did not show evidence of delamination.

### 3.4. Characterization of the films

#### 3.4.1. SEM

Fig. 14 shows the SEM image of the aCTi1 system before and after electrochemical evaluation. It can be observed that the film follows the surface morphology of the substrate which is a common characteristic of

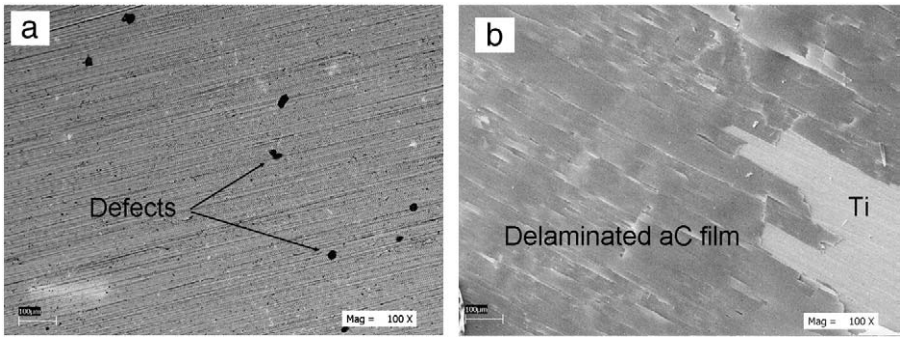


**Fig. 14.** SEM images of the aCTi1 system a — before and b —after electrochemical evaluation showing clear delamination of the a-C film.

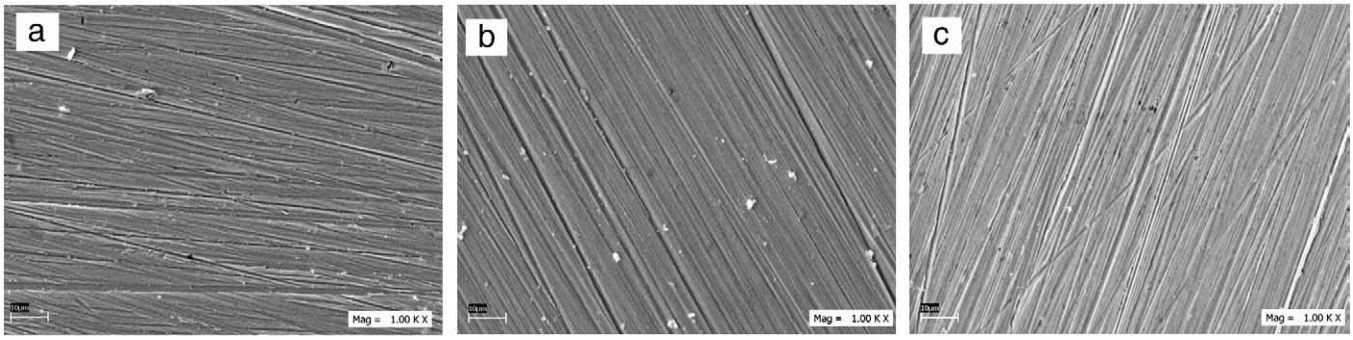


**Fig. 15.** SEM images of a — aCTi2, b — aCTi3 and c —SS, after electrochemical evaluation. The magnification in the three figures is 1000× and the scale is 10 μm.

the magnetron sputtering deposits but several defects are observed at the deposit. After the electrochemical evaluation the a-C film from the aCTi1 system was delaminated as was confirmed by energy dispersive spectroscopy (EDS), while the Ti underlayer remained. Fig. 15 shows both the aCTi2 and aCTi3 samples after electrochemical evaluation, where no signal of delamination nor localized attack is observed. In this figure we introduced the bare substrate for comparison after the electrochemical evaluation.

### 3.4.2. Raman

Fig. 16 shows the similarity between the Raman spectra of the a-C films deposited on a silicon substrate and of the aCTi2 system. Raman spectroscopy of amorphous carbon films have been extensively used to classify the samples, i.e. to distinguish between diamond-like and graphite-like characteristics. As mentioned in the introduction, the a-C films studied in this work are graphite-like in nature and their physical properties have been reported in previous works [25]. The present Raman spectra were taken to demonstrate that the film characteristics of the single a-C sample are the same as that of the double-layer samples, i.e. no modifications in the a-C properties are introduced by the Ti buffer layer.

### 3.4.3. Porosity index (P)

The porosity of PVD coatings has been extensively studied by a number of research groups using electrochemical techniques. The equation introduced by Tato and Landolt [26] defines a porosity index as simple as the anodic current density ratio of the coated substrate to the uncoated substrate. Nevertheless, more precise definitions include the polarization resistance and the anodic Tafel slope, as shown in the following equation [26–28]:

$$P = (R_{pm} / R_p) 10^{-|\Delta E_{corr}| / \beta_a} \quad (1)$$

where $P$ is the total coating porosity, $R_{pm}$ is the polarization resistance of the bare stainless steel, $R_p$ is the polarization resistance of the coating, $\beta_a$ is the anodic Tafel slope of the bare stainless steel and $\Delta E_{corr}$ is the difference in corrosion potential between the coated and bare substrate. The determination of the coatings porosity is essential to determine their corrosion resistance. The electrochemical determination of the coatings porosity is based on the fact that the pores in the coating provide a passage for the exposed substrate to react with the electrolyte. However, absolute porosity is not obtained, but a parameter which is someway proportional to the real pore fraction. Polarization curves obtained in this paper were used to determine the coating porosity index by the use of Eq. (1) taking parameters from Table 3 and the results are summarized in Table 4. According to these, the porosity index decreased in the following order aCTi1 > Ti3 > aCTi2 > aCTi3. The high porosity index obtained for sample aCTi1 explains the delamination that took place after electrochemical polarization as was previously described by the polarization curve and confirmed later by SEM.

**Table 4**
Porosity index obtained by the use of Eq. (1) with the parameters from the polarization curves.

| Sample | $P$ |
|---|---|
| Ti1 | 0.2160 |
| Ti2 | 0.4920 |
| Ti3 | 0.2796 |
| aCTi1 | 0.4412 |
| aCTi2 | 0.1942 |
| aCTi3 | 0.0975 |

The porosity estimated from Eq. (1) is not always suitable, due to the coating properties, but also some researchers have shown that this method overestimates the porosity [29]. A different approach is to use the results obtained from EIS [28,29]: where the polarization resistance in Eq. (1) is taken as the sum of all resistances representing the processes occurring during the impedance experiment, which in this case are $R_1$ and $R_2$, as described in Section 3.2 Since EIS measurements contains information as a function of the immersion time, $R_1$ and $R_2$ values at initial exposure describe the existence of intrinsic pores in the coating. As the time increased, the $R_p$ values describe the pore evolution in time. The $R_p$ as a function of time for the samples Ti1, Ti2 and Ti3 is shown in Fig. 17a. Both Ti2 and Ti3 showed a steady increment in $R_p$, while nearly no variation was observed for the Ti1 sample. The increment in $R_p$ suggested that a passivation process was taking place at the thicker Ti layers. For the aCTi systems shown in Fig. 17b, a very low $R_p$ was obtained for the aCTi1 in

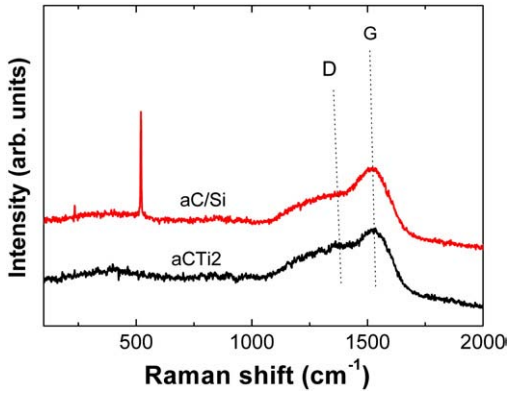


**Fig. 16.** Raman spectra showing the signature of a graphite-like amorphous carbon sample for the a-C sample deposited on Si substrate and the carbon of the aCTi2 double-layer system.

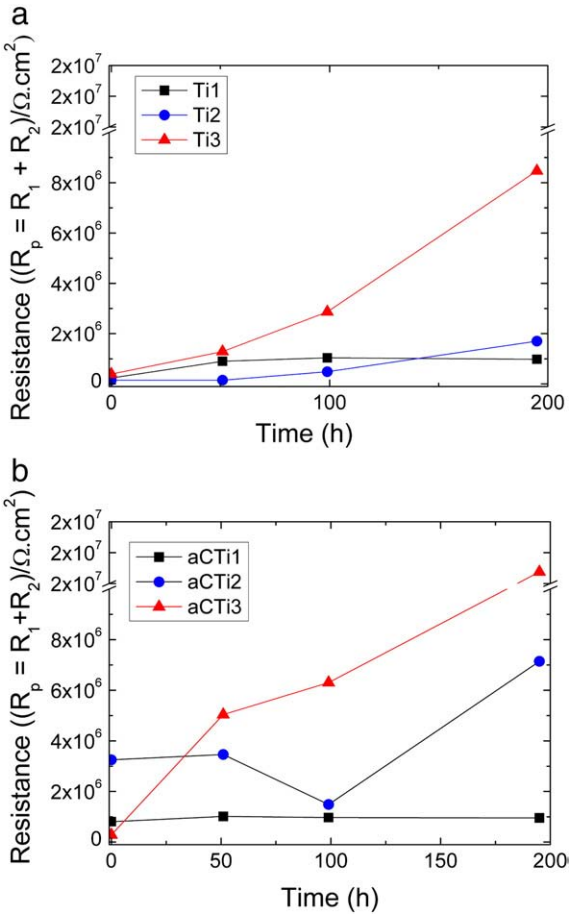


**Fig. 17.** Total resistance ($R_p = R_1 + R_2$) as a function of the immersion time estimated from the EIS analysis. a — Ti/SS system and b — aCTi/system.

**Table 5**
Porosity index determined by EIS data.[a]

| Sample | t, h | P |
|---|---|---|
| Ti1 | 3 | 0.522 |
| | 51 | 0.219 |
| | 99 | 0.196 |
| | 195 | 0.219 |
| Ti2 | 3 | 1.396 |
| | 51 | 1.270 |
| | 99 | 0.425 |
| | 195 | 0.091 |
| Ti3 | 3 | 0.430 |
| | 51 | 0.166 |
| | 99 | 0.063 |
| | 195 | 0.016 |
| aCTi1 | 3 | 0.094 |
| | 51 | 0.211 |
| | 99 | 0.087 |
| | 195 | 0.219 |
| aCTi2 | 3 | 0.039 |
| | 51 | 0.166 |
| | 99 | 0.109 |
| | 195 | 0.117 |
| aCTi3 | 3 | 0.501 |
| | 51 | 0.033 |
| | 99 | 0.025 |
| | 195 | 0.012 |

[a] $E_{corr}$ were used upon stable potential measurements, $R_p = R_1 + R_2$ from Table 2.

agreement to the trend observed for the Ti1 sample in Fig. 17a. On the other hand, a clear increment in the $R_p$ vs. time plot for both aCTi2 and aCTi3 samples was observed. The increasing $R_p$ can be the result of the combination of the accumulation of corrosion products in the pores (closing the pores) and to the passivation of the Ti buffered layer, which leads to the larger $R_p$ values at 195 h. Comparing the porosity index values shown in Table 4 with the trends in the $R_p$ of Fig. 17, it might be seen that the lower $P$ corresponds to the samples showing a larger slope in the $R_p$ vs. time plot. Moreover, the use of $R_1 + R_2$ from EIS analysis can be used to obtain the associated porosity using Eq. (1), and the results are shown in Table 5.

A third approach to study porosity in PVD coatings is the use of the EIS parameters, such as, $R_{pore}$, $R_{ct}$ and $C_{dl}$ or equivalently the $Q$ of the CPE2 of the EC models, which are related to the $R_1$, $R_2$ and $C_2$, respectively. The $R_{pore}$ is the resistance to current flow through the pores and is given by [29,30].

$$R_{pore} = \rho l / PA \quad (2)$$

where $l$ is the average pore length and is equivalent to the coating thickness, $A$ is the surface area exposed to the electrolyte, $P$ is the porosity of the coating and $\rho$ is the resistivity, which depends on the solution, size and shape of the defects. From this equation, it is clear that the porosity is inversely proportional to $R_{pore}$; so the greater the $R_{pore}$, the smaller the porosity. In Table 2, the evolution in time of $R_{pore}$ for the different samples is shown following the column $R_1$. The first value of the aCTi3 sample is not included since during the first 3 h of exposure, this system did not show the second low-frequency time constant, which is due to the ($R_{pore}$, $C_{coat}$) parallel circuit, suggesting a non-open porosity.

*3.4.4. Relationship between EIS and potentiodynamic polarization (PP) technique*

A correlation between the EIS results and the PP technique is not easy since each technique describe different processes. However, from the analysis of both data we can reach to similar conclusions when proper parameters are compared. The best Ti/a-C system was described by EIS as the system having the larger magnitude and increasing $R_1 + R_2$ as a function of time. This corresponds in the potentiodynamic test to the sample having both larger $R_p$ and anodic Tafel slope ($\beta_a$), while the lower current density. From Fig. 17, which refers to the $R_1 + R_2$ values, and Table 3 that contains the Tafel and $R_p$ values, we can conclude that the aCTi3 system gives the better corrosion resistance.

## 4. Conclusions

The corrosion behavior of double-layered PVD Ti/a-C coated medical grade stainless steel has been studied through the modeling of the EIS spectra at different times of exposure to 0.89% NaCl solution, which simulates body fluid conditions. The obtained parameters of the circuit elements were used to select the Ti/a-C thickness ratio that gives better performance.

1. At the first three hours of immersion, EIS spectra from most coated substrates present two time constants clearly distinguish in the phase vs. frequency spectra. The only exception was the aCTi3 system (thickness ratio: 530/240), which shows one time constant. As immersion time increases, the low-frequency peak was clearly distinguished for all samples. This signal represents the electrochemical response of the localized corrosion at the pores. However, the fact that the $|Z|$ remained nearly unchanged during the whole exposure time (up to 195 h) suggested that no major damage or delamination of the coatings occurred.
2. Analysis of the EIS modeling parameters demonstrated that the system having lower porosity and therefore a better corrosion resistance was the aCTi3 system. This trend was confirmed by SEM observation of the surface morphology after the electrochemical tests and also is in good agreement with the Tafel analysis of the polarization curves and the porosity index obtained.

## Acknowledgments

The project was supported by DGAPA PAPIT IN102907 and CONACYT P45833. D. Turcio-Ortega gratefully acknowledges CONACYT for posdoctoral fellowship. Authors wish to thank Thyssenkrupp Mexinox for AISI 316 samples, H. Zarco for electronic assistance and, J. A. Toledo-Antonio and M. A. Cortés-Jácome (Instituto Mexicano del Petróleo) for running the Raman spectra.

## References

[1] M.L. Morrison, R.A. Buchanan, P.K. Liaw, C.J. Berry, R.L. Brigmon, L. Riester, H. Abernathy, C. Jin, R.J. Narayan, Diam. Relat. Mater. 15 (2006) 138.
[2] C.M. Mcnie, D.C. Barton, E. Ingham, J.L. Tipper, J. Fisher, M.H. Stone, J. Mater. Sci.: Mater. Med. 11 (2000) 163.
[3] O.O. Ajayi, B. Shi, M.J. Soppet, A. Erdemir, H. Liang, G.R. Fenske, Tribol. Trans. 48 (2005) 190.
[4] T.R. Green, J. Fisher, J.B. Matthews, M.H. Stone, E. Ingham, J. Biomed. Mater. Res. 53 (2000) 490.
[5] A.W. Schaffer, A. Pilger, C. Engelhardt, K. Zweymueller, H.W. Ruediger, J. Toxicol.-Clin. Toxicol. 37 (1999) 839.
[6] R. Hauert, Tribol. Int. 37 (2004) 991.
[7] A. Grill, Diam. Relat. Mater. 12 (2003) 166.
[8] R.H. Wei, G. Dearnaley, J. Arps, Surf. Coat. Technol. 196 (2005) 1.
[9] V.M. Tiainen, Diam. Relat. Mater. 10 (2001) 153.
[10] J. Stallard, D. Mercs, M. Jarratt, D.G. Teer, P.H. Shipway, Surf. Coat. Technol. 177 (2004) 545.
[11] S.E. Rodil, R. Olivares, H. Arzate, S. Muhl, Diam. Relat. Mater. 12 (2003) 931.
[12] S.E. Rodil, R. Olivares, H. Arzate, Biomed. Mater. Eng. 15 (2005) 101.
[13] A. Zeng, E. Liu, S. Zhang, S.N. Tan, P. Hing, I.F. Annergren, J. Gao, Thin Solid Films 426 (2003) 258.
[14] B. Tomcik, S.C. Seng, B. Balakrishnan, J.Y. Lee, Diam. Relat. Mater. 11 (2002) 1409.
[15] P.D. Maguire, J.A. McLaughlin, T.I.T. Okpalugo, P. Lemoine, P. Papakonstantinou, E.T. McAdams, M. Needham, A.A. Ogwu, M. Ball, G.A. Abbas, Diam. Relat. Mater. 14 (2005) 1277.
[16] R. Schlesinger, M. Bruns, H.J. Ache, J. Electrochem. Soc. 144 (1997) 6.
[17] R. Hubler, Surf. Coat. Technol. 119 (1999) 1116.
[18] M. Stuber, S. Ulrich, H. Leiste, A. Kratzsch, H. Holleck, Surf. Coat. Technol. 119 (1999) 591.
[19] C.L. Liu, M. Xu, W. Zhang, S.H. Pu, P.K. Chu, Diam. Relat. Mater. 17 (2008) 1738.
[20] C. Liu, Q. Bi, A. Matthews, Surf. Coat. Technol. 163 (2003) 597.
[21] D. Turcio-Ortega, S.E. Rodil, S. Muhl, Mater. Sci. (Medziagotyra) 14 (2008) 15.
[22] G. Okamoto, Corros. Sci. 13 (1973) 471.

[23] G.T. Wu, C.S. Wang, X.B. Zhang, H.S. Yang, Z.F. Qi, P.M. He, W.Z. Li, J. Electrochem. Soc. 146 (1999) 1696.
[24] C. Fonseca, F. Vaz, M.A. Barbosa, Corros. Sci. 46 (2004) 3005.
[25] A.C. Ferrari, J. Robertson, Phys. Rev. B. Condens. Matter Mater. Phys. 61 (2000) 14095.
[26] W. Tato, D. Landolt, J. Electrochem. Soc. 145 (1998) 4173.
[27] S. Maeng, L. Axe, T.A. Tyson, P. Cote, Surf. Coat. Technol. 200 (2006) 5767.
[28] S.H. Ahn, J.H. Lee, H.G. Kim, J.G. Kim, Appl. Surf. Sci. 233 (2004) 105.
[29] C. Liu, Q. Bi, A. Leyland, A. Matthews, Corros. Sci. 45 (2003) 1257.
[30] C. Liu, Q. Bi, A. Leyland, A. Matthews, Corros. Sci. 45 (2003) 1243.